Journal of Hydrology 389 (2010) 168–176

Contents lists available at ScienceDirect

Journal of Hydrology

journal homepage: www.elsevier.com/locate/jhydrol

Comparative calculation of suspended sediment loads with respect to hysteresis effects (in the Petzenkirchen catchment, Austria)

A. Eder [a,*], P. Strauss [a], T. Krueger [b,1], J.N. Quinton [b]

[a] Federal Agency for Water Management, Institute for Land and Water Management Research, Pollnbergstr. 1, 3252 Petzenkirchen, Austria
[b] Lancaster Environment Centre, Lancaster University, UK

ARTICLE INFO

Article history:
Received 13 November 2009
Received in revised form 19 May 2010
Accepted 30 May 2010

This manuscript was handled by L. Charlet, Editor-in-Chief with the assistance of Georgia Destouni, Associate Editor

Keywords:
Turbidity
Suspended sediment
Agricultural catchment
Water quality
Hysteresis

SUMMARY

Streams in intensively used agricultural catchments are frequently characterised by high transport of suspended solids during rainfall events. Due to a high variability in runoff, the sediment concentration relationship during and between different events and various hysteresis effects, instantaneous sediment concentrations and event loads are difficult to calculate. We tested the applicability of turbidity measurements for calculating instantaneous sediment concentrations and loads in a small agricultural catchment in Austria. We calibrated quasi-continuous turbidity measurements using additional water sampling and employed these calibrated sediment concentrations as benchmark sediment concentrations. Four different methods to calculate instantaneous sediment concentrations were tested on 19 events. A generalized rating curve approach resulted in a considerable bias for both event specific sediment concentrations and total sediments loads. Fitting of event-specific rating curves still misrepresented instantaneous sediment concentrations for the different events, but gave load estimations that were in a range of 5% of the benchmark values. Two approaches accounting explicitly for hysteresis exhibited the best fit and provided load estimations that were in a range of 0–1% deviation to the benchmark sediment concentrations. Nevertheless, several limitations to the hysteresis model approach were identified. Testing the various hysteresis effects against other event parameters such as total rainfall amount, maximum rainfall intensity and initial soil water content revealed interactions to these parameters that could predefine parameter values of the hysteresis model approach.

1. Introduction

Streams in intensively used agricultural catchments are frequently characterised by increased transport of suspended solids during rainfall events, which may affect stream water quality considerably. Most of the annual sediment transport usually takes place during a few events (Kronvang et al., 1997), and thus the short-term dynamics of storm events are important in sediment loading.

Traditionally, these dynamics are characterised by empirical relationships between suspended sediment concentration (ssc) and discharge. These relationships are normally not homogenous in time, neither within nor between events. This causes a large scatter of ssc–discharge data pairs, which can often be explained by short- (within events) and long-term (between events) hysteresis effects (Walling and Teed, 1971). However, hysteresis is usually not taken into account in load estimation techniques. Nevertheless, it has been suggested that the hysteresis effect, and in particular its shape, may be an important indicator of different processes of runoff, location of sediment sources and sediment transport (Krueger et al., 2009; Seeger et al., 2004; Terajima et al., 1997; Williams, 1989). To account for the hysteresis effect of sediment concentration within single events, Krueger et al. (2009) introduced an empirical hysteresis model based on a concept used by House and Warwick (1998) to describe solute dynamics in rivers.

To identify within-event sediment behaviour, discontinuous water sampling or, more common in recent years, continuously measuring turbidity devices are employed (Lewis, 1996; Brasington and Richards, 2000; Stubblefield et al., 2007; Wass and Leeks, 1999). It has been shown that quasi-continuous turbidity recording may avoid significant uncertainty due to interpolation and extrapolation of low-frequency measurements (Grayson et al., 1996; Lewis, 1996) and to allow the investigation of the short-term dynamics of sediment transport (Kronvang et al., 1997; Stubblefield et al., 2007; Brasington and Richards, 2000; Nistor and Church, 2005; Chikita et al., 2002). However, problems in deriving a relationship between turbidity and ssc exist. Particularly, variations in the response of turbidity probes due to differences in particle size, sediment mineralogy and the colour of dissolved organic material (Gippel, 1995) as

* Corresponding author. Tel.: +43 7416 52108 73; fax: +43 7416 52108 80.
E-mail addresses: alexander.eder@baw.at (A. Eder), t.krueger@uea.ac.uk (T. Krueger).
[1] School of Environmental Sciences, University of East Anglia, Norwich NR4 7TJ, UK.

0022-1694/$ - see front matter © 2010 Elsevier B.V. All rights reserved.
doi:10.1016/j.jhydrol.2010.05.043

well as their sensitivity to clogging of the measurement window have been reported (Gurnell, 1987).

The aim of this paper is threefold: (1) we test the applicability of turbidity measurements for calculating continuous sediment concentrations in a stream draining a small agricultural catchment in Austria; (2) we compare five methods of estimating sediment concentrations to highlight hysteresis effects and their importance for identifying runoff generation processes; and (3) we assess the significance of hysteresis for estimating catchment sediment loads.

2. Materials and methods

2.1. Catchment description

The Petzenkirchen catchment (Fig. 1) is situated in the western part of Lower Austria and it has a size of 64 ha.

The climate can be characterised as humid with a mean annual temperature of 9.3 °C and a mean annual rainfall of 716 mm. Temperature, rainfall and rainfall intensity have their peak during summertime. The elevation of the catchment ranges from 268 to 323 m above sea level (a.s.l.) with a mean slope of 8%. The form factor of the catchment (width/length) is 0.3, while the river density (length of river in km/area of catchment in km^2) is 0.8. The dominant soil types are Cambisols and Planosols (FAO, 1998) with medium to poor infiltration capacities. Due to shallow low permeability soil and the use of the catchment area as agricultural land, sub-surface drainage systems were installed in the 1950s. The drainage systems influence both discharge and sediment concentration behaviour in the stream. The estimated drainage area from the drainage system is about 15% of the total catchment and can be divided into two bigger drainage systems in the southwestern part of the creek and four smaller drainage systems on the northeastern part (Fig. 1). Additionally, the upper most 25% of the stream length were piped in the 1950s to enlarge the agricultural production area. At present, 87% of the catchment area is arable land, 5% is used as pasture, 6% is forested and 2% is paved.

2.2. Instrumentation

Discharge, suspended sediment concentration and turbidity were monitored at the outlet of the Petzenkirchen catchment (Fig. 1). Discharge was measured every minute, indirectly with a calibrated H-flume in combination with a pressure transducer (OTT PS 1). The H-flume was self-made after instructions in BOS (1974) and had a maximum flow capacity of 400 l s^{-1}. The flow calming section upstream of the measuring point had a length of 3 m. Water samples (ws) were taken with an automatic suction sampler (Manning S 4040) at set intervals (see below) triggered by increasing flow rates (starting from 9.1 l s^{-1}). The inlet of the suction tube was placed into the small swirl zone directly after

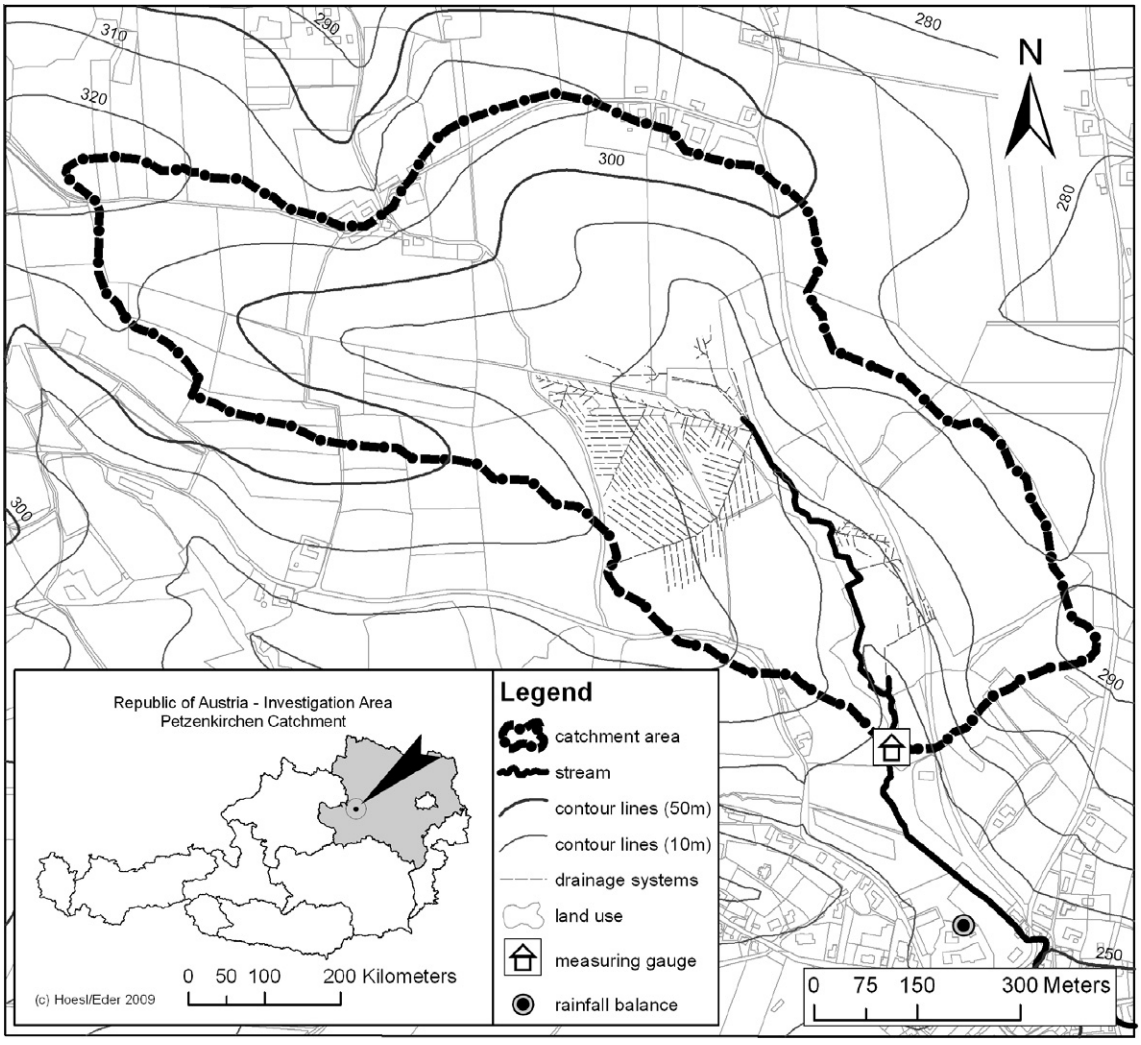

Fig. 1. Petzenkirchen catchment.

the flume to ensure good mixing of the sampled volume. The volume of the swirl zone is approximately 500 l, which means a mean residence time of 250 s at low flow conditions. The sampler minimises mixing of samples by a 17 s of purge cycle before and after the filling of the samples. Within an event, samples were taken at constant time intervals ranging from 3.75 min to 24 h. The intervals were chosen in advance of an event according to the weather forecast to ensure an optimal sampling distribution. In addition, manual sampling took place once per week. All water samples were filtered through 0.45 μm membrane filters and oven-dried to obtain sediment concentrations (ssc_{ws}) gravimetrically. An in-stream turbidity device (WTW: ViSolid 700 IQ) was used to collect quasi-continuous turbidity data at 3 min intervals. The measurement range for this device was from 0 to 25 g l^{-1} with a resolution of 0.01 g l^{-1}.The device uses a scattered light measurement, which records the reflectance of total suspended solids. The reflectance was transformed into suspended sediment concentration (turb) using the default calibration equation, supplied by the manufacturer. The turbidity probe was installed into the swirl zone next to the suction tube of the automatic sampler to guarantee both similar measuring conditions and required distance of the optical sensor to fixed surrounding structures.

Rainfall was recorded with a rainfall balance (OTT Pluvio) situated about 200 m away from the catchment outlet. Readings were taken every 0.1 mm of rainfall.

Surrogate measurements of catchment soil water content was obtained from TDR-probes located in a lysimeter station close to the catchment at the beginning of events.

2.3. Event separation

An automated recursive digital filter (Nathan and McMahon, 1990; Arnold et al., 1995) was applied to the whole time series to identify periods of direct flow. Due to noisy discharge data, a moving average filter with a window size of 5 min was first used to smooth the data. The equation of the recursive digital filter is given by

$$q_t = \beta \cdot q_{t-1} + (1+\beta)/2 \cdot (Q_t - Q_{t-1}) \quad (1)$$

where q_t is the filtered quick response (event water) at time step t and Q_t is the original stream flow. The value of the filter parameter β was manually set to 0.95 after visual data inspection.

For our study, we defined an 'event' as beginning when stream discharge increased above base flow, to the time when only base flow contributed to discharge, although there may still have been increased base flow sediment concentrations. Subsequently, the maximum discharge of an event had to be at least 5 l s^{-1}. The difference between the maximum discharge and the antecedent discharge had to be greater than 2 l s^{-1} and the maximum turbidity had to reach values above 100 mg l^{-1} to define an event. These constraints were necessary to avoid a large number of low-flow events with low suspended sediment concentrations in the stream water.

2.4. Suspended sediment concentration (ssc)

Quasi-continuous suspended sediment concentrations were calculated comparing five different methods:

(a) Calibration of turbidity data against ssc_{ws}: → ssc_{tu}

Gippel (1995) states that, in general, the best correlations were obtained in areas where sediment properties were likely to be relatively constant (oceanic environments and small catchments), where field instruments were used, and where the concentration of suspended sediments covered a wide range. The Petzenkirchen catchment fulfils all of the requirements. Both linear and exponential relations between water samples and turbidity were tested via statistical regression analysis.

Results of this method were used as benchmark, when the different methods were compared.

(a) Rating curve generated from all ssc_{ws}–discharge data pairs: → ssc_R

A power-law rating curve is usually employed to describe this kind of relationship (e.g. in Campbell and Bauder, 1940) for annual catchment sediment load estimation. Following Asselman (2000), we did not transform the power-law logarithmically to avoid transformation bias. Instead, the power-law function was fitted to all ssc_{ws}–discharge data pairs using non-linear least-square regression. The rating curve has the form

$$ssc_R = a \cdot q^b \quad (2)$$

where a and b are the fitting parameters, ssc_R is the suspended sediment concentration and q represents the discharge.

(a) Rating curve generated from ssc_{ws}–discharge data pairs for single individual events: → ssc_{RE}

The power-law function was fitted to individual events in the same way as in (b) to account for the potential of rating curve heterogeneity between events.

(a) Hysteresis model after Krueger et al. (2009) with discharge records and ssc_{ws} as input for individual events: → ssc_{Hws}

Krueger et al's model was tested to include the hysteresis behaviour of discharge–ssc relationships during single events. Krueger et al. introduced a term incorporating the steepness of the rising and falling limbs of the hydrograph during single events to characterise the hysteresis effect of sediment dynamics. They modified Eq. (2) to

$$ssc_H = a \cdot q^b + c \cdot dq/dt \quad (3)$$

where c is an additional fitting parameter and dq/dt is the steepness of the hydrograph (for similar use of dq/dt see Paustian and Beschta (1979), Terajima et al. (1997), House and Warwick (1998) and Ide et al. (2008)). This allows to account for sediment peaks that arrive at the catchment outlet in advance (clockwise) or after (counter-clockwise) the hydrograph peak. Eq. (3) was fitted to discharge–ws data by non-linear least-square regression for individual events.

(a) Hysteresis model after Krueger et al. (2009) with discharge records and calibrated turbidity records (ssc_{tu}) as input for individual events: → ssc_{Htu}

The hysteresis model (Eq. (3)) was fitted to the calibrated turbidity–discharge data pairs for single events in the same way as in (d) to display possible differences induced by the availability of data pairs (low-resolution ssc_{ws} versus high-resolution ssc_{tu}).

The validity of all model fits was quantified by the Nash–Sutcliffe efficiency (Nash and Sutcliffe, 1970) with respect to the calibrated turbidity record (ssc_{tu}) as a benchmark. Please note that for this study no explicit consideration of possible data uncertainties in a model rejectionist framework (such as in Krueger et al. (2009)) was attempted. Instead, the five different methods of calculating ssc were compared in a classic non-linear optimisation setting, which allows gauging their relative merits. However, a future study to fully assess the uncertainties in these methods is envisaged.

2.5. Catchment sediment load (CSL)

Measured and calculated suspended sediment concentrations were used to estimate catchment sediment load for the observed events and to compare the different methods of generating continuous suspended sediment concentrations.

3. Results and discussion

3.1. Event separation

The mean flow during the study period (2005–2008) was 3.9 l s^{-1}, while the minimum discharge was 0.2 l s^{-1} and the maximum flow was 293 l s^{-1}. The highest discharge ever observed was above 400 l s^{-1} in 2002. In total, event separation led to 82 runoff events with rainfall, discharge and turbidity data available. In 19 of the 82 events, suspended sediment data were available as well. These 19 events formed the database for subsequent analyses. Table 1 gives an overview of the characteristics of these events.

The method used for event separation was determined as appropriate, because temporal extension of the events showed only minor effect on sediment load calculations due to very low sediment concentrations before and after the defined events. However, the definition of the beginning and ending of an event is important, especially for sediment load calculations on event basis.

3.2. Suspended sediment concentrations

Turbidity records, transformed with the default calibration equation to suspended sediment concentrations (turb) as described above, ranged from 0 to 25 g l^{-1}, the upper detection limit of the turbidity probe. Maximum suspended sediment concentration of the automatic water sampler (ssc_{ws}) was 27.3 g l^{-1}, but this was a unique value. ssc_{ws} and turb were linearly correlated (Pearson $r = 0.91$) (Fig. 2).

The slope of 0.631 ± 0.024 (95% confidence intervals) of the linear regression in Fig. 2 indicates that the internal default calibration equation of the turbidity probe was not sufficient to deliver absolute suspended sediment concentrations. This is not surprising since turbidity devices are known to have some limitations, i.e. the requirement of simultaneous water sampling for calibration (Lewis, 1996; Brasington and Richards, 2000) and regular cleaning of the optical window Gurnell (1987). Furthermore, the turbidity

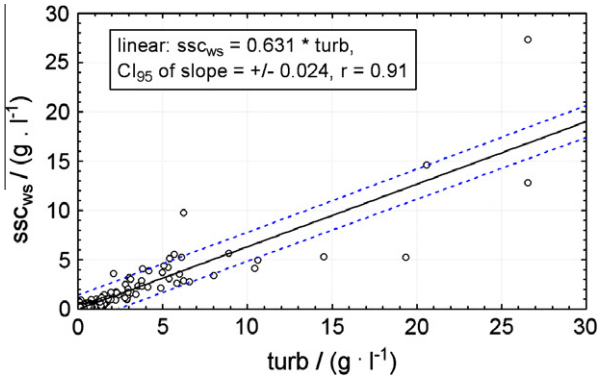

Fig. 2. Relationship between suspended sediment concentration of the water sampler (ssc_{ws}) and default turbidity values (turb).

records required a plausibility check, manual data correction and calibration. However, by using turbidity devices we could avoid the typical representational problems of automated water sampling (Fig. 3) i.e. sampling intervals that are either too large to resolve sediment peaks or too short leading to an exhaustion of sampling bottles in advance of the peak.

Obviously the total suspended sediment concentration consists of either material, which has been eroded from somewhere in the catchment including the stream bank or material, which has been re-suspended during increase of flow. Unfortunately, we are not able to distinguish these sources at present.

3.3. Rating curves

In general, the relationship between discharge and sediment concentration data showed a large scatter (Fig. 4). A number of variables may influence the variation of this relationship: (i) rainfall characteristics like duration, intensity, time to peak and spatial distribution; (ii) initial catchment conditions like soil water content and its spatial distribution, land use, management practises and stadium of plant development; (iii) flow characteristics at the event beginning of an event like discharge and sediment concentration. The fit to the scattered data was consequently characterised by a low correlation coefficient of 0.32 (Fig. 4) and led to overestimated suspended sediment concentrations for most of the events (Fig. 5 – left) and an underestimation of suspended

Table 1
Event number (No.), date of event, event duration (duration in h), event maximum discharge (q_{max} in l s^{-1}), rainfall amount (I in mm), maximum rainfall intensity within 10 min (I_{10} in mm h^{-1}), initial soil water content at 10 cm depth (θ_{10} in %) and estimated catchment sediment load (CSL_{tu} in kg).

No.	Date	Duration (h)	q_{max} I (μs^{-1})	I (mm)	I_{10} (mm μh^{-1})	θ_{10}	CSL_{tu} (kg)
E1	09.03.2006	37.3	16.2	5.6	2.4	35.5	148
E2	28.03.2006	19.2	37.3	17.3	4.8	35.3	724
E3	17.05.2006	2.8	8.4	4.2	8.4	26.4	4
E4	02.06.2006	23.8	21.9	26.9	6.6	35.6	126
E5	18.09.2006	3.1	18.4	23.7	76.2	22.5	231
E6	01.01.2007	16.7	11.3	13.0	7.2	35.4	83
E7	18.01.2007	20.3	38.8	26.1	10.2	35.0	1006
E8	27.02.2007	17.8	14.3	12.9	3.0	35.8	177
E9	23.03.2007	21.7	24.0	16.4	9.6	35.4	213
E10	05.09.2007	25.9	60.6	66.2	6.6	28.4	1369
E11	07.11.2007	24.8	36.2	19.3	9.0	34.1	377
E12	21.04.2008	5.1	19.7	19.4	21.6	29.1	69
E13	03.06.2008	15.6	17.7	27.2	22.8	25.6	90
E14	25.06.2008	3.6	8.4	10.9	24.6	24.8	24
E15	26.06.2008	3.4	10.4	12.3	31.8	24.5	26
E16	12.07.2008	1.8	50.1	13.8	48.0	24.0	1609
E17	20.07.2008	7.2	7.3	14.5	11.4	26.3	73
E18	23.07.2008	18.0	10.8	25.7	7.8	28.4	146
E19	24.07.2008	7.8	59.2	12.8	9.0	34.0	706

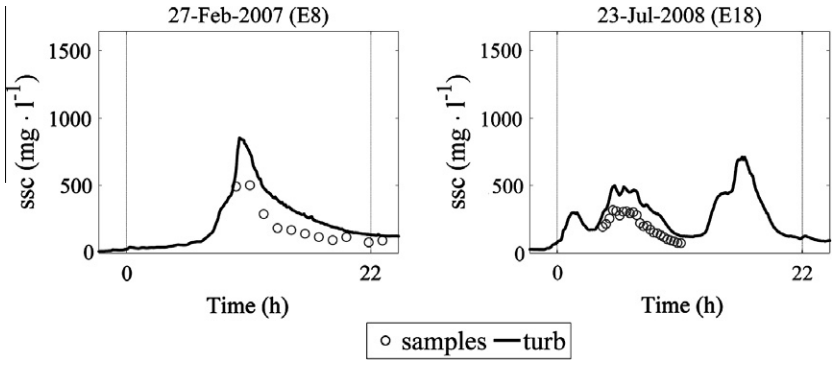

Fig. 3. Missing sediment peak due to large sampling intervals on the left and use of all sampling bottles before the end of a long lasting event (right).

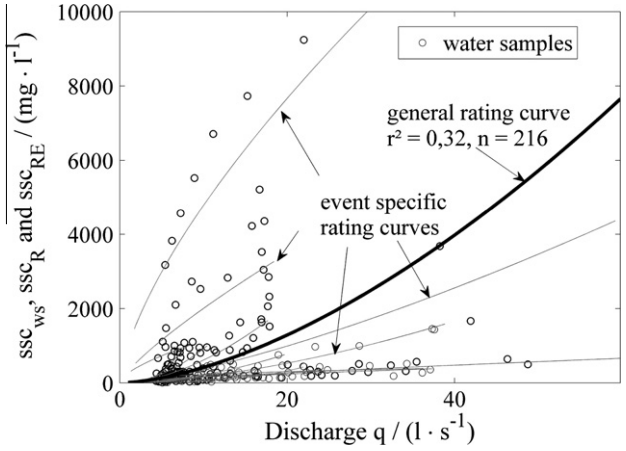

Fig. 4. Suspended sediment concentration of the water samples (ssc_{ws}) against discharge, general rating curve generated from all water samples – discharge data pairs (ssc_R) and event-specific rating curves (ssc_{RE}).

sediment concentration for a few heavy storm events (Fig. 5 – right). However, these events tend to contribute most to annual sediment loads and therefore annual loads are often underestimated using these forms of average rating curves (Kronvang et al., 1997).

Fitting event-specific rating curves (Fig. 4), demonstrates the enormous variability of sediment–discharge relationships within the same catchment. Table 2 provides information on model parameters, correlation coefficients of the model fits (with respect to ssc_{ws}) and model efficiencies (with respect to the ssc_{tu}) for each event. The correlation coefficients of the event-specific rating curves ranged from 0.04 to 0.99. It should be noted that some of these fits were extremely poor, whereas the validity of other fits might have been positively biased by the low number of water samples and the timing of sampling during an event. Nevertheless, applying event-specific rating curves resulted in higher correlation coefficients overall compared to the general rating curve.

The model efficiencies (E_R and E_{Re}) of the simulated suspended sediment concentrations (ssc_R and ssc_{Re}) with respect to the calibrated turbidity record (ssc_{tu}) depended on the correlation coefficients of the model fit to the water samples and the magnitudes of hysteresis. The mostly negative values of the Nash–Sutcliffe coefficient for the general rating curve (E_R) confirm that it cannot be used to calculate suspended sediment concentrations for single events. Better results were obtained with event-specific rating curves, illustrated by raised efficiencies (E_{Re}), although half of the events yielded E_{Re} values below 0.5. There is, therefore, scope for model improvement.

3.4. Hysteresis model – ssc

The hysteresis model was applied to both water samples (ssc_{ws}) and calibrated turbidity data (ssc_{tu}) sets. Table 3 gives the model parameters, the model efficiencies and the actual direction of hysteresis.

Taking in account the hysteresis effect in suspended sediment calculations led to increasing efficiencies ($E_{H,ws}$) in nine of nineteen events compared to the event-specific rating curves. In six cases, efficiency did not change and in four events efficiency declined, which indicates some limitations of the hysteresis model's approach. No improvement could be obtained for events with a low number of data points, which do not represent the full dimension of the hysteresis (E1), multi-peak events with different numbers of

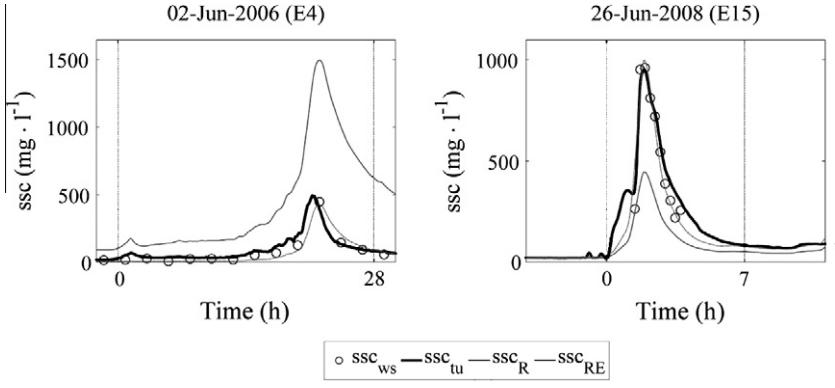

Fig. 5. Calculated suspended sediment concentrations (ssc_R – general rating curve, ssc_{RE} – event-specific rating curve) compared to suspended sediment concentration of the water samples (ssc_{ws}) and calibrated turbidity records (ssc_{tu}).

Table 2
Model parameters of Eq. (2) (a and b), number of data points (n), correlation coefficients of the model fits to the water samples (r_R and r_{RE}) and Nash–Sutcliffe efficiencies with respect to the turbidity record for both general (E_R) and event specific (E_{RE}) rating curves.

	General rating curve					Event-specific rating curves				
	a_R	b_R	n_R	r_R	E_R	a_{RE}	b_{RE}	n_{RE}	r_{RE}	E_{re}
E1	9.90	1.63	216	0.57	−32.75	0.01	3.72	3	1.00	−0.14
E2	9.90	1.63	216	0.57	−271.56	23.49	0.77	9	0.54	−0.30
E3	9.90	1.63	216	0.57	−12.46	3.09	1.67	6	0.63	0.36
E4	9.90	1.63	216	0.57	−18.24	0.05	2.96	12	0.97	0.62
E5	9.90	1.63	216	0.57	−1.39	317.67	0.80	17	0.55	0.10
E6	9.90	1.63	216	0.57	0.41	11.77	1.25	6	0.21	0.76
E7	9.90	1.63	216	0.57	−4.66	3.86	1.64	11	0.97	0.70
E8	9.90	1.63	216	0.57	0.26	1.22	2.11	10	0.47	0.29
E9	9.90	1.63	216	0.57	−37.83	2.00	1.64	14	0.75	0.69
E10	9.90	1.63	216	0.57	−193.53	23.69	0.81	16	0.80	0.52
E11	9.90	1.63	216	0.57	−20.56	89.07	0.41	5	0.27	0.45
E12	9.90	1.63	216	0.57	−0.43	3.14	1.84	10	0.96	0.88
E13	9.90	1.63	216	0.57	0.90	10.60	1.76	24	0.76	0.92
E14	9.90	1.63	216	0.57	−0.54	262.50	0.64	6	0.50	0.40
E15	9.90	1.63	216	0.57	0.17	11.11	1.92	10	0.95	0.88
E16	9.90	1.63	216	0.57	−1.37	999.24	0.68	12	0.85	0.21
E17	9.90	1.63	216	0.57	−0.43	3.45	2.77	13	0.81	0.70
E18	9.90	1.63	216	0.57	0.17	12.64	1.45	24	0.39	0.02
E19	9.90	1.63	216	0.57	−1.77	16.71	1.36	5	0.84	0.37

Table 3
Model parameters of Eq. (3) (a–c), number of data points (n), correlation coefficients of the hysteresis model fits to ssc_{ws} (r_{Hws}) and ssc_{tu} (r_{Htu}), Nash–Sutcliffe efficiencies with respect to the turbidity record for both hysteresis model applications (E_{Hws} and E_{Htu}) and direction of the hysteresis loop (cl – clockwise, ac – counter clockwise, 8 – eight-shaped and – no hysteresis).

	Hysteresis model water samples (ssc_{ws})						Hysteresis model turbidity data (ssc_{tu})					Direction of hysteresis
	a_{Hws}	b_{Hws}	c_{Hws}	n_{Hws}	r_{Hws}	E_{hws}	a_{Htu}	b_{Htu}	c_{Htu}	n_{Htu}	E_{Htu}	
E1	0.01	3.84	−989	3	1.00	−1.21	1.35	1.80	2435	2236	0.91	cl
E2	1.46	1.56	3187	9	0.92	0.19	37.67	0.66	2885	1151	0.51	cl
E3	5.17	1.39	−168	6	0.83	0.57	4.29	1.49	−222	166	0.59	8
E4	0.04	3.04	1390	12	0.99	0.89	0.59	2.08	1678	1426	0.95	cl
E5	342.89	0.79	−1268	17	0.59	−1.26	809.65	0.41	−2720	186	0.46	ac
E6	290.63	−0.18	2049	6	0.97	−1.03	1.60	2.26	62	1001	0.96	–
E7	4.31	1.61	−286	11	0.98	0.68	2.83	1.68	1770	1216	0.85	cl
E8	0.16	2.89	1925	10	0.67	0.39	1.28	2.29	3288	1066	0.80	cl
E9	0.53	2.08	1412	14	0.86	0.81	2.44	1.58	1226	1301	0.85	cl
E10	23.41	0.82	−75	16	0.80	0.51	65.94	0.58	451	1556	0.75	cl
E11	0.21	2.28	2273	5	0.70	0.17	1.73	1.68	−80	1486	0.99	–
E12	2.93	1.87	70	30	0.96	0.87	5.00	1.68	−134	306	0.89	8
E13	10.39	1.77	−192	24	0.76	0.91	8.21	1.79	268	936	0.97	8
E14	153.00	0.92	−1021	6	0.97	0.71	66.03	1.40	−568	216	0.85	8
E15	9.59	1.98	−244	10	0.96	0.86	33.06	1.43	−123	206	0.95	8
E16	941.64	0.70	−756	12	0.87	0.32	2946.66	0.44	−3013	111	0.72	ac
E17	1.64	3.15	−4240	13	0.91	0.68	1.90	3.26	−2778	431	0.88	ac
E18	11.58	1.48	4975	24	0.93	0.24	16.73	1.45	3677	1081	0.50	cl
E19	4.99	1.71	1561	5	1.00	0.27	13.42	1.32	1237	466	0.89	cl

sediment and discharge peaks (E6, E11, E19), and noisy events without smoothing the data (see Fig. 6).

Examples for valid and failed fits of the hysteresis model are displayed in Fig. 6. The diagrams on the left side show discharge, calibrated turbidity records (ssc_{tu}), the suspended sediment concentrations of the water samples (ssc_{ws}) and the calculated suspended sediment concentrations of the hysteresis model (ssc_{Hws}). On the right diagram, the corresponding hysteresis loops can be seen. Limitations of the modelling approach can be classified into not enough data (Fig. 6b), different number of discharge and sediment peaks (Fig. 6c), noisy data and a conspicuous sagging of subsequent sediment peaks compared to discharge peaks in multi-peak events.

The highest Nash–Sutcliffe efficiencies were obtained when the hysteresis model was fitted to calibrated turbidity data. The higher number of data pairs, which resolved the shape of hysteresis better, led to efficiencies (E_{Htu}) ranging from 0.50 to 0.99. Even multi-peak events with small loops inside another hysteresis loop were predicted well, although the validity of fit decreased slightly due to smaller subsequent sediment peaks compared to the discharge peaks. This underlines the importance of a sufficient quantitative data set and continuous monitoring when dynamic behaviour of sediment transport is the point of interest.

In case the hysteresis model fitted the data reasonably well, parameter c of Eq. (3) directly reflected the behaviour of sediment concentration during an event, i.e. the direction and extent of the hysteresis loop (Table 3). Positive values of c correspond to clockwise hysteresis (cl), while high negative c values are an indication for counter clockwise loops (ac), and c values around zero correspond to an eight-shaped form (8) or nearly no hysteresis (–). Nine events showed a clockwise hysteresis (E1, E2, E4, E7, E8, E9, E10; E18, E19) and five events showed an eight-shaped hysteresis (E3, E12, E13, E14, E15). Only in three cases (E5, E16, E17), a counter clockwise loop was observed. Two events showed nearly no hysteresis (E6, E11).

In a next step, we evaluated values for c against various event characteristics. Fig. 7 shows correlations between c and different event characteristics and its corresponding hysteresis direction.

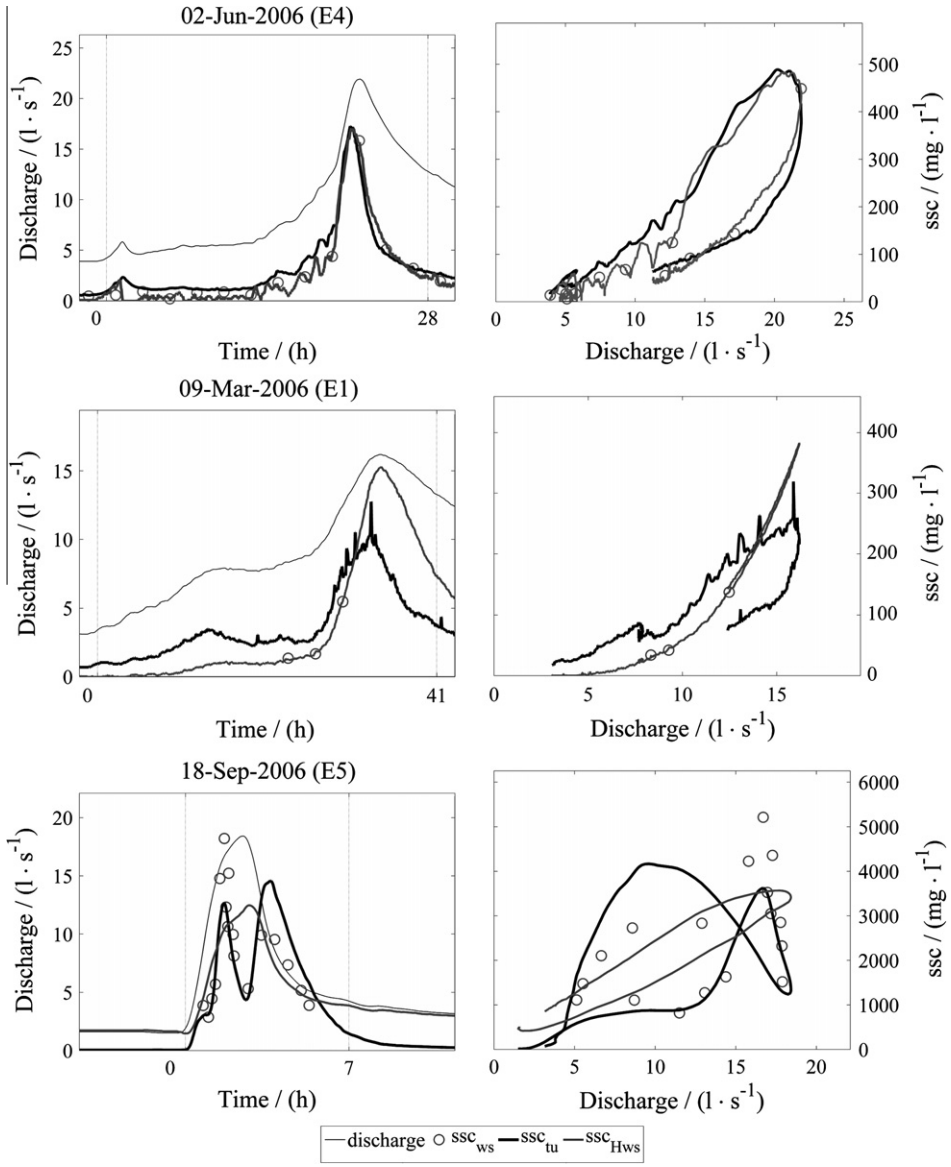

Fig. 6. Discharge, suspended sediment concentration of the water samples (ssc_{ws}), calibrated turbidity data (ssc_{tu}) and calculated suspended sediment concentrations of the hysteresis model (ssc_{Hws}) on the left and the corresponding hysteresis loops on the right. (a) Good simulation, (b) not enough data, (c) different number of discharge and sediment peaks.

Clockwise hysteresis required rainfalls with long duration (Brasington and Richards, 2000) and low intensity, high total runoff and high initial soil moisture. Counter clockwise hysteresis occurred at small events with high rainfall intensity and very dry soil conditions. This can be explained by the significantly higher flood wave celerity compared to the flow velocity that carries the bulk of suspended sediment (Williams, 1989; Brasington and Richards, 2000). Counter clockwise hysteresis in events with long duration, observed by Seeger et al. (2004), was not detected in the Petzenkirchen catchment.

In case of long lasting events with low intensities, wave velocity was not fast enough to appear in advance of the bulk of sediment. On the contrary, the peak of sediment concentration appeared in front of the discharge peak. A possible explanation of clockwise hysteresis is the exhaustion of easily available sediments close to the stream (Williams, 1989). At low intensity rainfall events, only saturation excess runoff is expected. It is in areas at the bottom of the slope, close to the stream, that contribute first to discharge due to higher initial soil water contents. Therefore, sediment coming from these areas would contribute first to sediment discharge. A further source of early sediment may be the stream bed (Williams, 1989; Kronvang et al., 1997; Lenzi and Marchi, 2000), where sediments are available due to increasing shear stress. Additionally, the stream bank could contribute to the sediment source (Kronvang et al., 1997) from sediments deposited at the end of former events. A further continuation of rainfall may cause an increasing area to contribute to discharge and sediment delivery. However, the easily available sediments close to the stream may already be exhausted, leading to reduced sediment input from areas that contribute since the beginning of the event.

An explanation for the variable extent of hysteresis may be the heterogeneity of rainfall characteristics and different initial conditions in terms of soil moisture, discharge, land use, management practices and plant development. For example, areas with lower soil water contents, perhaps with actively growing crops, will contribute later and less water in comparison to those with higher water contents, for example area after harvest.

Eight-shaped hysteresis combined both directions of hysteresis and occurred at low total amounts of runoff, medium rainfall intensities and medium soil water contents. All events with

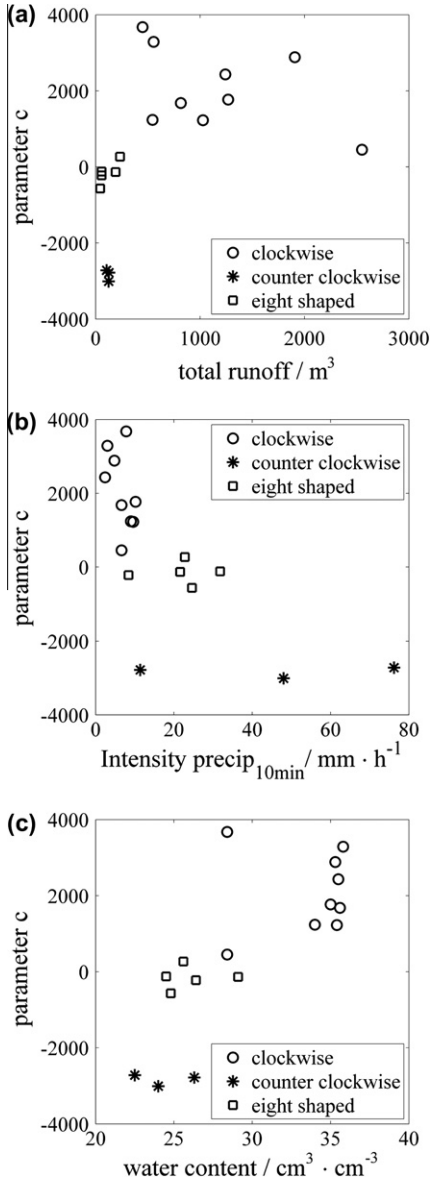

Fig. 7. Correlation between parameter *c* of the hysteresis model (Eq. (3)) and total rainfall amount (a), maximum rainfall intensity within 10 min, (b) and initial soil water content (c), together with the corresponding hysteresis direction of the event (clockwise, counter clockwise and eight-shaped).

eight-shaped hysteresis had the clockwise loop at low discharges followed by a counter clockwise hysteresis. Seeger et al. (2004) mentioned the same phenomena. Possible explanations can be: (i) a sediment flush from the streambed and its banks, (ii) a delayed contribution of a sub-catchment, (iii) storage in small basins and their later connection after filling or (iv) influences of drainage. Kronvang et al. (1997) measured a sediment contribution from drainages of up to 69% in an arable catchment. Its temporal delay is caused by the passage through the soil, even when preferential flow paths through the soil exist.

Further investigations of the contribution of drainages on sediment transport and the influence of soil moisture and vegetation will be done when more events have been recorded.

3.5. Catchment sediment load (CSL)

Calculations of catchment sediment loads for single events employing the different model approaches are given in Table 4.

Table 4
Measured (CSL_{tu} – calibrated turbidity data) and calculated (CSL_R – general rating curve, CSL_{RE} event-specific rating curve, CSL_{Hws} – hysteresis model fitted to water samples, CSL_{Htu} – hysteresis model fitted to turbidity data) catchment sediment loads on event basis.

	CSL_{tu}	CSL_R	CSL_{RE}	CSL_{Hws}	CSL_{Htu}
Event loads in kg					
E	148	638	172	200	148
E2	724	4809	610	645	722
E3	4	11	4	4	4
E4	126	548	110	117	124
E5	231	68	245	257	234
E6	83	124	65	84	83
E7	1006	2812	1171	1157	1007
E8	177	255	103	99	177
E9	213	946	197	198	213
E10	1369	10,411	1166	1181	1373
E11	377	1787	334	367	378
E12	69	119	67	67	69
E13	90	71	107	107	89
E14	24	5	29	26	24
E15	26	11	23	23	26
E16	1609	379	1258	1254	1622
E17	73	20	54	51	72
E18	146	120	106	110	146
E19	706	1627	1039	1138	708
Σ events	7200	24,760	6859	7083	7217

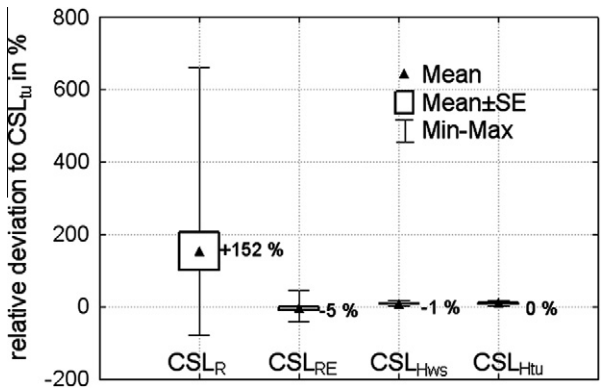

Fig. 8. Relative errors of catchment sediment load for the tested calculation methods (CSL_R – general rating curve, CSL_{RE} – event-specific rating curve, $CSLH_{ws}$ – hysteresis model applied to water samples, CSL_{Htu} – hysteresis model applied to calibrated turbidity data) compared to measured catchment sediment load (CSL_{tu}).

Calibrated turbidity records (ssc_{tu}) produced event loads between 4 kg and 1609 kg, which will again be used as a benchmark. Calculations with the general rating curve (ssc_R) led to a mean overestimation of 152% with a maximum of 660% and a minimum of −78% compared to ssc_{tu} for the same events (Fig. 8). Nearly no differences in prediction of sediment load occurred between the event specific loading function (ssc_{RE}) and the hysteresis model (ssc_{Hws}). Values varied from 4 to 1258 kg and from 4 to 1254 kg, respectively. The variation of suspended loads compared to CSL_{tu} ranged from 47% to −42% and from 61% to −44%, with a mean difference of −5% and −1%, respectively. Although ssc_{Hws} was calculated with higher accuracy compared to ssc_R, there is no indication for a better prediction of total suspended sediment load. This seems to be due to a systematic averaging out of the deficiencies of the ssc_{RE} model described above over a full event. The most accurate results were obtained with the application of the hysteresis model using the calibrated turbidity data (ssc_{Htu}), with maximum calculation errors between 1% and −1%.

4. Conclusions

We used quasi-continuous turbidity measurements and additional water sampling as the best available representation of instantaneous sediment concentrations in the stream draining the Petzenkirchen catchment, Austria. However, the necessity of probe calibration indicated that even with the effort of additional water sampling there is still considerable uncertainty associated with the estimation of in-stream sediment concentrations.

Transport of suspended sediment in-streams underlies a wide range of influencing factors. Their variability caused enormous variation of the ssc – flow relationship in this study and therefore biased ssc calculations considerably when a general rating curve approach was used. We obtained better results when using rating curves on an event basis, but omitting hysteresis effects still misrepresented instantaneous ssc calculations.

Of the 19 events that were analysed, nine showed a clockwise hysteresis, five were eight-shaped and three followed a counter clockwise loop. For two events, nearly no hysteresis was detected. We used the model parameter *c* of the Krueger et al. (2009) hysteresis model to classify the direction and extent of hysteresis. Variable rainfall intensities, antecedent soil water content and total runoff amounts were identified as most relevant for the hysteresis direction. High *c* values, i.e. large counter clockwise hysteresis loops, were caused by long enduring events with low intensities and higher initial soil moisture. Small but intense events and drier soil conditions entailed counter clockwise hysteresis and therefore high negative *c* values. Eight-shaped hysteresis loops are mixed forms that happened during events with medium rainfall intensity and medium initial soil water content, but total runoff had to be very low.

Although several limitations to successfully applying the hysteresis model have been identified, parameter *c* of the Krueger et al. (2009) model provided additional information about the hysteresis behaviour of suspended sediment concentrations in the study catchment. Specifically, we found that the value of parameter *c* directly reflected direction and extent of the hysteresis loop, depending on various event characteristics.

In contrast, for the calculation of total loads of suspended sediment, application of a single event rating approach was already sufficient to obtain reliable event loads with respect to the observed benchmark turbidity data. However, application of a general rating curve led to mean deviations of more than 150%, making this a highly questionable solution for calculating reliable sediment loads, even when calculating annual sediment loads.

References

Arnold, J.G., Allen, P.M., Muttiah, R., Bernhardt, G., 1995. Automated base flow separation and recession analysis techniques. Ground Water 33, 1010–1018.

Asselman, N.E.M., 2000. Fitting and interpretation of sediment rating curves. Journal of Hydrology 234, 228–248.

Bos, 1974. Discharge Measurement Structures, The Working Group on Small Hydraulic Structures, Wageningen University and Research Centre.

Brasington, J., Richards, K., 2000. Turbidity and suspended sediment dynamics in small catchments in the Nepal Middle Hills. Hydrological Processes 14, 2559–2574.

Campbell, F.B., Bauder, H.A., 1940. A rating-curve method for determining silt-discharge of streams. Transactions of the American Geophysical Union 21, 603–607.

Chikita, K.A., Kemnitz, R., Kumai, R., 2002. Characteristics of sediment discharge in the subarctic Yukon River, Alaska. Catena 48, 235–253.

FAO, ISRIC and ISSS, World Reference Base of Soil Resources: World Soil Resources Report 84, Rome, 1998.

Gippel, C.J., 1995. Potential of turbidity monitoring for measuring the transport of suspended solids in streams. Hydrological Processes 9, 83–97.

Grayson, R.B., Finlayson, B.L., Gippel, C.J., Hart, B.T., 1996. The potential of field turbidity measurements for the computation of total phosphorus and suspended solids loads. Journal of Environmental Management 47, 257–267.

Gurnell, A.M., 1987. Suspended sediment. In: Gurnell, A.M., Clark, M.J. (Eds.), Clacio-Fluvial Sediment Transfer. Wiley, Chichester, pp. 305–354.

House, W.A., Warwick, M.S., 1998. Hysteresis of the solute concentration/discharge relationship in rivers during storms. Water Resources 32, 2279–2290.

Ide, J.H., Haga, H., Chiwa, M., Otsuki, K., 2008. Effects of antecedent rain history on particulate phosphorus loss from a small forested watershed of Japanese cypress (*Chamaecyparis obtusa*). Journal of Hydrology 352 (3–4), 322–335.

Kronvang, B., Laubel, A., Grant, R., 1997. Suspended sediment and particulate phosphorus transport and delivery pathways in an arable catchment, Gelbaek stream, Denmark. Hydrological Processes 11, 627–642.

Krueger, T., Quinton, J.N., Freer, J., Macleod, C.J.A., Bilotta, G.S., Brazier, R.E., Butler, P., Haygarth, P.M., 2009. Uncertainties in data and models to describe event dynamics of agricultural sediment and phosphorus transfer. Journal of Environmental Quality 38 (3), 1137–1148.

Lenzi, M.A., Marchi, L., 2000. Suspended sediment load during floods in a small stream of the dolomites (Northeastern Italy). Catena 39, 267–282.

Lewis, J., 1996. Turbidity controlled suspended sediment sampling for runoff-event load estimation. Water Resources Research 32, 2299–2310.

Nash, J.E., Sutcliffe, J.E., 1970. River flow forecasting through conceptual models. Part I. A discussion of principles. Journal of Hydrology 10, 282–290.

Nathan, R.J., McMahon, T.A., 1990. McMahon, evaluation of automated techniques for base flow and recession analyses. Water Resources Research 26, 1465–1473.

Nistor, C.J., Church, M., 2005. Suspended sediment transport regime in a debris-flow gully on Vancouver Island, British Columbia. Hydrological Processes 19, 861–885.

Paustian, S.J., Beschta, R.L., 1979. Suspended sediment regime of an Oregon coast range stream. Water Resources Bulletin 15 (1), 144–154.

Seeger, M., Errea, M.-P., Begueria, S., Arnaez, J., Marti, C., Carcia-Ruiz, J.M., 2004. Catchment soil moisture and rainfall characteristics as determinant factors for discharge/suspended sediment hysteretic loops in a small headwater catchment in the Spanish Pyrenees. Journal of Hydrology 288, 299–311.

Stubblefield, A.P., Reuter, J.E., Dahlgren, R.A., Goldman, C.R., 2007. Use of turbidometry to characterize suspended sediment and phosphorus fluxes in the Lake Tahoe basin, California, USA. Hydrological Processes 21, 281–291.

Terajima, T., Sakamoto, Nakai, Y., Kitamura, K., 1997. Suspended sediment discharge in subsurface flow from the head hollow of a small forested watershed, northern Japan. Earth Surface Processes and Landforms 22 (11), 987–1000.

Walling, D.E., Teed, A., 1971. A simple pumping sampler for research into suspended sediment transport in small catchments. Journal of Hydrology 13, 325–337.

Wass, P.D., Leeks, G.J.L., 1999. Suspended sediment fluxes in the Humber catchment, UK. Hydrological Processes 13, 935–953.

Williams, G.P., 1989. Sediment concentration versus water discharge during single hydrological events in rivers. Journal of Hydrology 111, 89–106.